

On the Reset of the Wind-Forced Decadal Kuroshio Extension Variability in Late 2017

BO QIU,^a SHUIMING CHEN,^a NIKLAS SCHNEIDER,^a EITAROU OKA,^b AND SHUSAKU SUGIMOTO^c

^a *Department of Oceanography, University of Hawai'i at Mānoa, Honolulu, Hawaii*

^b *Atmosphere and Ocean Research Institute, The University of Tokyo, Kashiwa, Japan*

^c *Department of Geophysics, Graduate School of Science, Tohoku University, Sendai, Japan*

(Manuscript received 4 April 2020, in final form 18 September 2020)

ABSTRACT: Decadal modulations of the Kuroshio Extension (KE) system between a stable and an unstable dynamic state in the western North Pacific have prevailed in the past three decades. This dominance of decadal variations is controlled by the negative feedback loop involving the wind-forced KE variability and its feedback onto the overlying extratropical storm tracks and the basin-scale surface wind field. The wind-forced decadal KE modulations were disrupted in August 2017 due to the development of the Kuroshio large meander south of Japan. By forcing the inflow KE paths northward and by avoiding overriding the shallow Izu Ridge, the Kuroshio large meander was able to compel the KE to change rapidly from the wind-forced, pre-existing, unstable state to a stable state. Following the large meander occurrence in late 2017, the stabilized KE change is found to affect the overlying storm tracks and the basin-scale wind field the same way as those generated by the wind-forced KE change prior to 2017. Given the consistent atmospheric response to both the large-meander-induced and wind-forced KE variability, we expect that the KE dynamic state will resume its decadal modulation after the phase reset relating to the 2017 large meander event.

KEYWORDS: Atmosphere-ocean interaction; Boundary currents; Climate prediction; Decadal variability; Mesoscale processes; Oceanic variability

1. Introduction

The Kuroshio has its origin in the northern branch of the North Equatorial Current (NEC) that flows westward and bifurcates off the Philippine coast near 12°N (Fig. 1). As it flows poleward, the Kuroshio gains progressively its volume transport and becomes a well-defined western boundary current (WBC) with a transport of ~ 15 Sv ($1 \text{ Sv} \equiv 10^6 \text{ m}^3 \text{ s}^{-1}$) when reaching the Luzon Strait (Lien et al. 2014). After passing by Taiwan, the Kuroshio enters the semi-enclosed East China Sea wherein its path is dynamically constrained by the steep continental slope. The Kuroshio enters the deep Shikoku basin through the Tokara Strait near 130°E and, due to the development of an offshore recirculation gyre, its eastward volume transport can reach up to 60 Sv (e.g., Imawaki et al. 2013). The Kuroshio exits the Shikoku basin by overriding the shallow Izu Ridge along 140°E and it is renamed the Kuroshio Extension (KE) after it enters the open North Pacific. With the enhancement from both the southern and northern recirculation gyres, the volume transport of the eastward-flowing KE has been observed to exceed 100 Sv (Wijffels et al. 1998; Qiu et al. 2008; Jayne et al. 2009).

Large-amplitude variability in the Kuroshio/KE system can be separated into three segments, each with distinct regional characteristics. The first segment lies in the latitudinal band east of Luzon and Taiwan between 18° and 25°N. As indicated in Fig. 1, this band has a high mesoscale eddy variability that extends eastward to the Hawaiian Islands across the western North Pacific Ocean. Mesoscale eddies along the 18°–25°N band have been observed to propagate westward with a typical

period of $O(100)$ days and a phase speed of about 0.1 ms^{-1} , and they are generated by baroclinic instability induced by the zonal velocity shear between the eastward-flowing Subtropical Countercurrent (STCC) in the surface layer and the westward-flowing NEC in the subsurface layer in the western North Pacific (Qiu 1999; Kobashi and Kawamura 2002; Cheng et al. 2017). After impinging upon the western boundary, the STCC mesoscale eddies have been detected to exert significant changes in the Kuroshio path and transport inside the East China Sea, as well as the Ryukyu Current that flows northward to the east of the Ryukyu Islands (e.g., Zhang et al. 2001; Gilson and Roemmich 2002; Ichikawa et al. 2004; Andres et al. 2008).

The second segment of enhanced Kuroshio variability appears in the deep Shikoku basin south of Japan. Constrained by the inflow via the narrow Tokara Strait and the need to override the meridionally oriented Izu Ridge along 140°E, the Kuroshio in the Shikoku basin is known for its bimodal path fluctuations between a nearshore straight path and an offshore meandering path (Kawabe 1995). During both of these two paths (commonly known as the “straight path” and “large meander path”), the Kuroshio exits the Shikoku basin via a relatively deep channel centered around 34°N along the shoaling Izu Ridge. In addition to these two preferred paths, the Kuroshio south of Japan can also exhibit a third path that loops southward over the shoaling Izu Ridge. The Kuroshio path fluctuations south of Japan are highly irregular and chaotic; the occurrence of the Kuroshio large meander (LM) shows no dominant periodicities, nor a preferred duration [for recent reviews, see Qiu and Miao (2000) and Usui et al. (2013)]. As will be explored in section 3 of this study, the dynamical causes underlying the bimodal Kuroshio path fluctuations in the Shikoku basin continues to be a topic of active research.

Corresponding author: Bo Qiu, bo@soest.hawaii.edu

DOI: 10.1175/JCLI-D-20-0237.1

© 2020 American Meteorological Society. For information regarding reuse of this content and general copyright information, consult the AMS Copyright Policy (www.ametsoc.org/PUBSReuseLicenses).

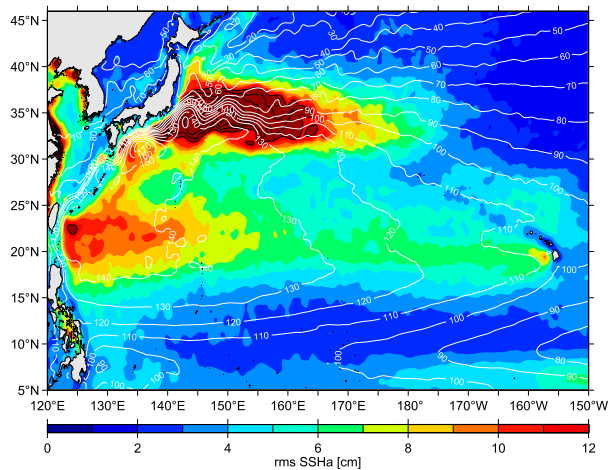


FIG. 1. Root-mean-square sea surface height variability in the western North Pacific based on high-pass filtered satellite altimeter data from January 1992 to February 2020. The high-pass filter has a half-power at 180 days. Regions where the rms variability exceeds 12 cm are indicated by black contours with an interval of 2 cm. White contours denote the mean SSH field by Rio et al. (2011).

Free from the constraint of coastal boundaries, the KE east of Japan constitutes the third high eddy variability segment. With the enhancement of its volume transport and horizontal shear, the KE has long been observed to be an eastward-flowing inertial jet accompanied by large-amplitude meanders and energetic pinched-off eddies (e.g., Mizuno and White 1983; Yasuda et al. 1992). One salient feature emerging from recent satellite and eddy-resolving ocean general circulation model simulations is that the KE exhibits well-defined decadal modulations between a stable and an unstable dynamic state (Qiu and Chen 2005, 2010; Taguchi et al. 2007; Ceballos et al. 2009; Sugimoto and Hanawa 2009; Sasaki et al. 2013; Pierini 2014; Bishop et al. 2015). For example, Fig. 2 shows that the KE paths were relatively stable in 1993–94, 2002–05, 2010–15, and 2018–19, based on merged satellite altimeter observations. In contrast, spatially convoluted paths prevailed during 1995–2001, 2006–09, and 2016–17. This decadal modulation of the KE system has persisted after the 1976–77 “climate shift” in the North Pacific (Qiu et al. 2014) and the basinwide wind stress curl variability associated with the Pacific decadal oscillations (PDOs; Mantua et al. 1997), or the North Pacific gyre oscillations (NPGOs; Di Lorenzo et al. 2008), has been identified as the external forcing that controls the phase change between the stable/unstable dynamic states.

Given their distinct characteristics, the oceanic circulation variability in these three segments of the North Pacific wind-driven WBC system has largely been explored separately in the past studies. The objective of our present study is to use the occurrence of the Kuroshio large meander in late 2017 to demonstrate that the variability in the aforementioned three segments are dynamically interconnected. To better understand the roles of the KE variability upon the overlying atmosphere, we argue that it is, in fact, critical to clarify the interactions among the mesoscale eddies from the STCC band,

the Kuroshio path fluctuations south of Japan, and the downstream KE variability in the open Pacific Ocean.

This paper is organized as follows. After describing the observational datasets in section 2, we examine in section 3 the KE dynamic state variability and its influence upon the overlying atmosphere. The negative feedback loop that enhances the decadal fluctuations in the extratropical ocean–atmosphere system of the North Pacific is reviewed. In section 4, the bimodal Kuroshio path fluctuations in the Shikoku basin are examined with a focus on the ongoing Kuroshio LM event that started in August 2017. In section 5, we address how the LM-induced KE dynamic state change affects the oceanic and overlying atmospheric circulation, and point to the reset of the negative feedback loop in the extratropical North Pacific ocean–atmosphere system by the 2017 LM occurrence. Discussion is provided in section 6 and section 7 summarizes the findings from the present study.

2. Observational datasets

To examine the surface oceanic circulation changes, we use the global sea surface height (SSH) dataset processed by Ssalto/Duacs and distributed by the Copernicus Marine and Environment Monitoring Service (CMEMS) (<https://marine.copernicus.eu/>). This dataset merges along-track SSH measurements from all satellite altimeter missions after October 1992 and has a 7-day temporal resolution and a $1/4^\circ$ spatial resolution. The data period analyzed in this study extends from January 1993 to December 2019.

To explore the subsurface circulation changes surrounding the KE jet, we utilize the conductivity–temperature–depth (CTD) surveys conducted by Japan Meteorological Agency (JMA) southeast of Japan on 28 February–11 March 2017 versus 2–12 March 2018. The CTD data have a vertical resolution of 1 dbar in the 2000-m upper ocean and can be accessed from https://www.data.jma.go.jp/gmd/kaiyou/db/vessel_obs/data-report/html/ship/ship.php.

To relate the oceanic variability to those at the air–sea interface and in the overlying atmosphere, we adopt the daily data from the European Centre for Medium–Range Weather Forecasts (ECMWF) ERA5 reanalysis product (<https://cds.climate.copernicus.eu/>). The ECMWF ERA-5 data have a spatial resolution of 0.25° and are available from January 1979 to present. To infer the location/baroclinicity of extratropical storm tracks, we follow Hoskins and Valdes (1990) and calculate the maximum Eady growth rate, $\sigma_{BI} = 0.31fN^{-1}\partial U/\partial z$, in the lower troposphere. Specifically, the vertical zonal wind shear $\partial U/\partial z$ and the static stability parameter N are evaluated using the ERA5 data between 700- and 850-hPa levels. To quantify the amplitude of extratropical storm-track activities, we follow Nakamura et al. (2002) and calculate the synoptic-scale (2–8 days) meridional transient eddy temperature fluxes $\langle v'T' \rangle$ from the hourly 850-hPa level ERA5 data.

3. KE dynamic state and its prediction/verification

There are several metrics to quantify the decadal variability of the KE system depicted visually in Fig. 2. Figure 3a, for

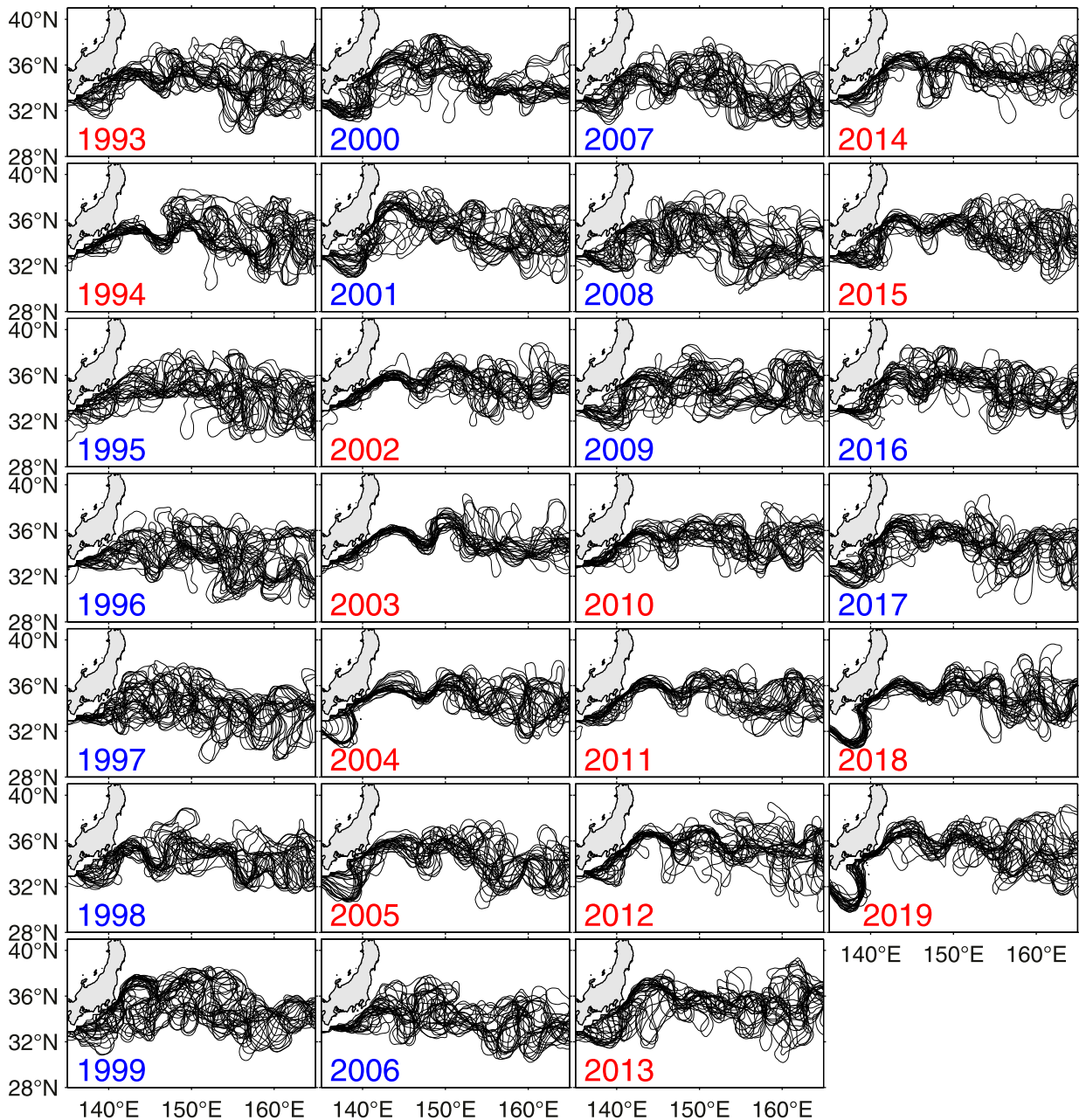


FIG. 2. Yearly paths of the Kuroshio and KE plotted every 14 days since 1993 based on satellite altimetry observations [for detailed path derivation, see Qiu and Chen (2005)]. Red (blue) labels denote years in which the KE is largely in a stable (unstable) dynamic state.

example, shows the KE path length integrated from 141° to 153° E. A short (long) path length here corresponds to a stable (unstable) KE dynamic state. Similarly, Figs. 3b and 3c show the surface eastward transport and latitudinal position of the KE averaged from 141° to 165° E, and Fig. 3d shows the strength of the KE's southern recirculation gyre based on the satellite altimeter SSH data of the past 27 years. In its stable dynamic state, the KE jet tends to have an intensified eastward transport, a northward latitudinal position, and an enhanced

southern recirculation gyre. The reverse is true when the KE jet switches to an unstable dynamic state. Given the close connections among the dynamic properties shown in Fig. 3, Qiu et al. (2014) combined these four time series (by reversing the sign of KE path length and averaging the four time series normalized by their respective standard deviations) and introduced the "KE index" to concisely represent the low-frequency changes of the KE system. As shown in Fig. 4a, a positive (negative) KE index is defined to represent a stable

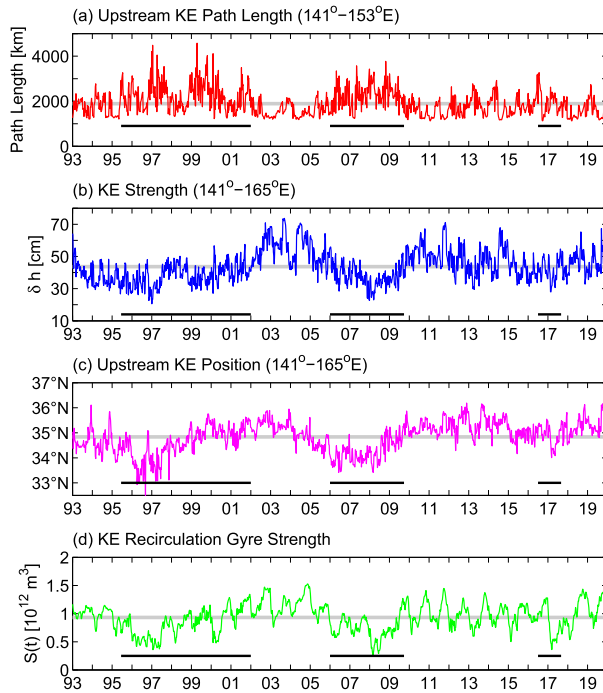


FIG. 3. Time series of (a) upstream KE path length integrated from 141° to 153°E, (b) SSH difference across the KE jet averaged from 141° to 165°E, (c) latitudinal position of the KE averaged from 141° to 165°E, and (d) intensity of the KE recirculation gyre. Thick black lines denote the periods when the KE is in an unstable dynamic state. For more details about the time series, see Qiu and Chen (2005).

(unstable) KE dynamic state. Statistically, the KE index is correlated favorably with the SSH anomaly signals averaged in the southern recirculation gyre region of 31°–36°N, 140°–165°E (Fig. 4b). This favorable correlation makes dynamical sense because a stable KE state is accompanied by an intensified southern recirculation gyre, hence a positive regional SSH anomaly.

Like all other extratropical WBCs, the Kuroshio/KE transport a significant amount of warmer tropical water poleward, providing a source of heat and moisture for the midlatitude atmosphere (Kelly et al. 2010). This source of oceanic heat/moisture has been demonstrated by many recent studies to help maintain the lower tropospheric baroclinicity and anchor the extratropical storm tracks (Nakamura et al. 2004; Minobe et al. 2008; Kwon et al. 2010; Booth et al. 2012; Small et al. 2014; Masunaga et al. 2016; Ma et al. 2016; Bishop et al. 2017; Parfitt and Seo 2018). Many data analysis studies in the past decades have examined the impact of the SST changes in the KE region on the atmospheric circulation across the midlatitude North Pacific basin (Frankignoul and Sennechael 2007; Qiu et al. 2007, 2017; Frankignoul et al. 2011; Taguchi et al. 2012; Smirnov et al. 2015; Ma et al. 2015; O'Reilly and Czaja 2014; Révelard et al. 2016). A consistent feature resulting from these analyses is that when the KE dynamic state is stable, increased surface turbulent (i.e., sensible + latent) heat fluxes

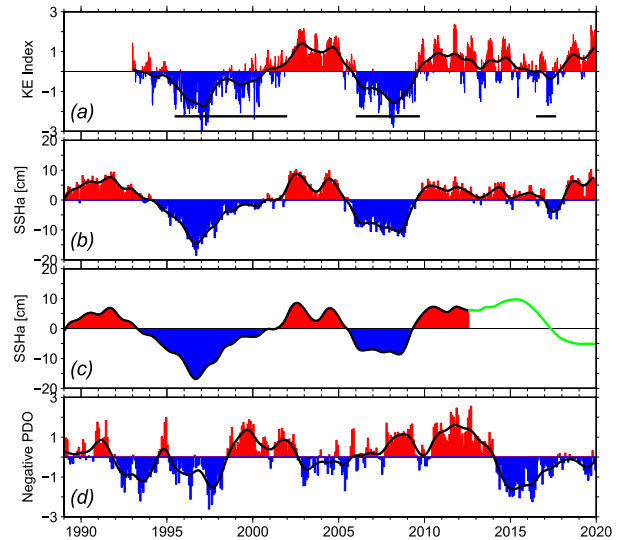


FIG. 4. (a) Time series of the KE index synthesized from the KE dynamical properties shown in Figs. 3a–d. (b) Time series of SSH anomalies averaged in the KE southern recirculation region of 31°–36°N, 140°–165°E. (c) As in (b), but for the SSH anomalies of 2013–19 (the green line) predicted based on the observed SSH data of 1989–2012. See Qiu et al. (2014) for derivations of the SSH anomaly time series and its prediction. (d) Time series of the negative PDO index (available from http://research.jisao.washington.edu/data_sets/pdo). Anomalies in (b)–(d) are relative to their respective 1989–2019 means and thick black lines in (a), (b), and (d) denote the time series after a low-pass filter that has a half-power at 6 months.

tend to emit from ocean to atmosphere along the poleward-shifted KE path (Fig. 5a; defined positive from ocean to atmosphere). This enhanced turbulent heat flux forcing results in northward migration/amplification of the extratropical storm tracks as can be inferred from the lower-tropospheric Eady growth rate and transient eddy ($\langle u'T' \rangle$) distributions shown in Figs. 5b and 5c. In connection with the meridional migration of storm tracks, the Ekman pumping velocity (w_{Ek}) field tends to similarly shift northward across the North Pacific basin (Fig. 5d).

Notice that the time-mean storm tracks follow roughly the $w_{\text{Ek}} = 0$ line denoted by the thick black contour in Fig. 5. This line is tilted southwest–northeast across the North Pacific basin due to the combined orographic constraint and diabatic oceanic forcing (Wilson et al. 2009). When the storm tracks migrate northward during the KE's stable state, a negative w_{Ek} anomaly band appears that straddles the time-mean $w_{\text{Ek}} = 0$ line (Fig. 5d). South of this band, the w_{Ek} anomalies turn positive because the northward migration of the wind system brings in weaker, subtropical-origin, negative w_{Ek} signals from the south. As a consequence, the anomalous w_{Ek} in the 31°–36°N band of the eastern North Pacific becomes positive. For the lower atmosphere, this positive w_{Ek} anomaly brings about enhanced regional rainfall over the eastern North Pacific (Ma et al. 2015). For the upper ocean, this leads to regional Ekman flux divergence and negative SSH anomalies in the eastern North Pacific Ocean. When these wind-forced negative SSH signals propagate westward into the KE region with a delay of

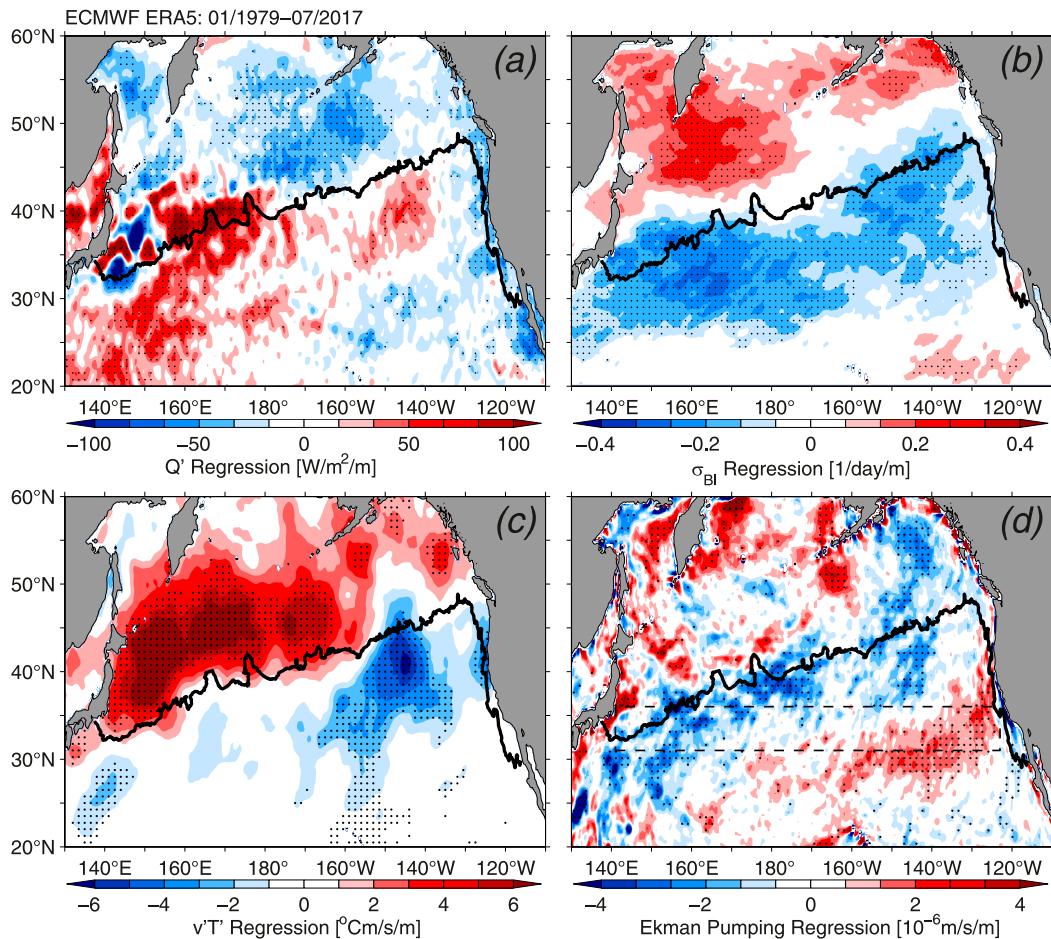


FIG. 5. (a) Regression coefficient between the surface turbulent heat flux anomaly field and the KE index of Jan 1979–Jul 2017 with the former lagging the latter by 2 months. (b) As in (a), but for the maximum Eady growth rate anomaly field at the 700–850-hPa level. (c) As in (a), but for the 2–8-day band-passed meridional transient eddy temperature flux anomaly field at the 850-hPa level. (d) As in (a), but for the w_{EK} anomaly field. In all figures, the thick black contour denotes the time-mean $w_{EK} = 0$ line and stippled areas indicate where the statistical significance exceeds the 90% confidence level based on Monte Carlo simulations [for detailed methodology, see Qiu et al. (2007)]. Dashed box in (d) indicates the 31°–36°N band where the Ekman pumping forcing impacts the KE dynamic state.

3–4 years, they work to weaken the southern recirculation gyre, shifting the KE jet southward to override the shallow Izu Ridge, and transforming the KE system to an unstable dynamic state (e.g., Qiu and Chen 2005; Taguchi et al. 2007). Once the KE system switches to its unstable state, the reverse of the atmospheric responses depicted in Fig. 5 takes place and a dynamic state transition to a stable state occurs following a delayed oceanic adjustment. Although the KE-induced basin-scale atmosphere response is weak in comparison with the internal atmospheric fluctuations (typically at 10%–15% level for the interannual and decadal signals), this ocean-to-atmosphere feedback loop provides a negative feedback mechanism that was argued by many recent studies to explain the enhanced decadal variability observed in the extratropical North Pacific ocean and atmosphere (Qiu et al. 2014; Smirnov et al. 2015; Na et al. 2018).

It is relevant to mention that many of the studies cited above have related the KE's dynamic state variability to the basin-wide wind forcing associated with the PDOs. As shown in Fig. 4d, there is a good correspondence between the negative PDO index and the KE index, or the recirculation gyre SSH signals, with the former leading the latter by 3 years and a correlation coefficient $r = 0.52$. A similar good correspondence also exists between the KE index and the NPGO index put forth by Di Lorenzo et al. (2008). Physically, this is not surprising because the KE dynamic state change is caused by the low-frequency surface wind stress fluctuations in the North Pacific basin that are encapsulated by leading climate indices, such as the PDO and the NPGO.

The aforementioned negative feedback loop provides not only a mechanism for explaining the enhanced decadal variability, but also a framework for predicting the KE dynamic state.

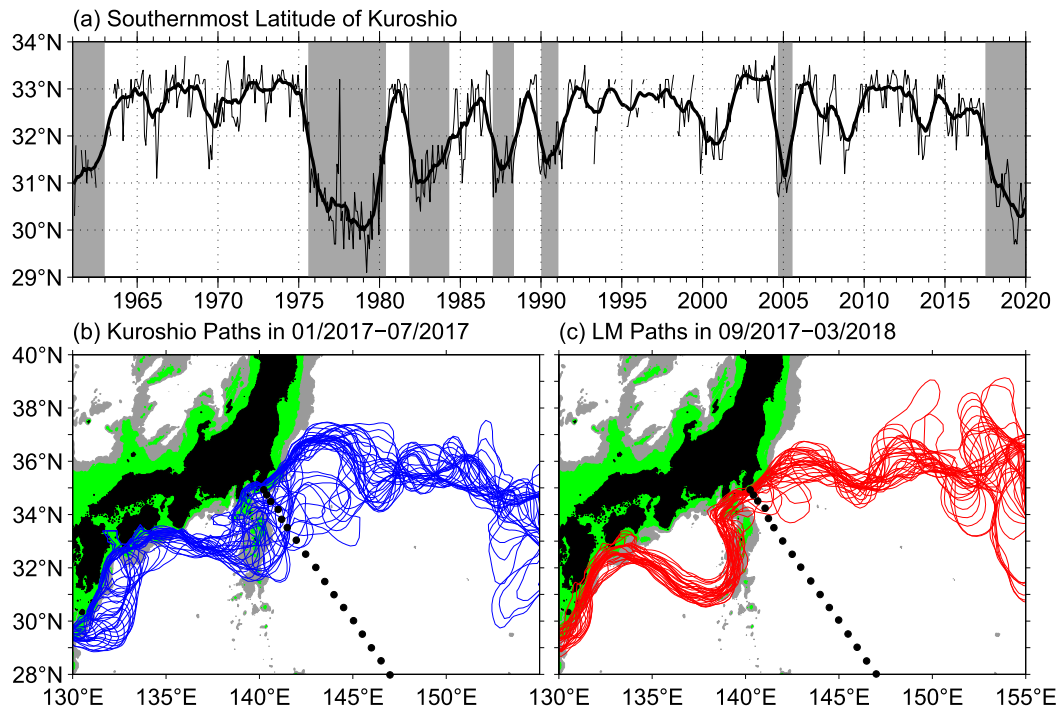


FIG. 6. (a) Time series of the monthly southernmost latitude of the Kuroshio south of Japan compiled by the Japan Meteorological Agency. Solid thick line shows the low-pass filtered time series after a 13-month running-mean average. Shaded periods with latitude $< 31.8^{\circ}\text{N}$ denote the large meander state of the Kuroshio. (b) Weekly Kuroshio/KE paths off Japan during January–July 2017. Black dots denote CTD stations by JMA cruise KS1702. (c) As in (b), but during September 2017–March 2018 and JMA cruise RF1802. Green (gray) shade denotes areas shallower than 500 (1500) m.

Relying on the slow oceanic baroclinic adjustment that carries the wind-forced SSH signals into the KE region and the basin-scale storm tracks and Ekman pumping field response to the changing KE dynamic state, we have attempted to forecast the SSH signals in the KE's recirculation region or, equivalently, the KE index for the 2013–22 period based on the observed SSH field of 2012 [see green line in Fig. 4c; replotted from Fig. 8 in Qiu et al. (2014)]. Compared to the observed SSH time series shown in Fig. 4b, it is interesting to note that the prediction did a good job in forecasting the positive-to-negative SSH change of the KE dynamic state in early 2017. The prediction, however, failed to forecast the abrupt reversal of the SSH signals to positive (i.e., stabilizing of the KE dynamic state) in late 2017.

4. The 2017 Kuroshio large meander event

What caused the “failure” of the predicted KE dynamic state in late 2017 based on the negative feedback loop between the KE and atmosphere storm track interactions? The answer is the occurrence of the Kuroshio LM that started in August 2017 in the upstream Shikoku basin. Figure 6a shows the monthly time series of the southernmost latitude of the Kuroshio south of Japan compiled by Japan Meteorological Agency based on combined 200-m water temperature measurements and satellite observations ([\[data.jma.go.jp/gmd/kaiyou/data/shindan/b_2/kuroshio_stream/kuroshio_stream.html\]\(http://data.jma.go.jp/gmd/kaiyou/data/shindan/b_2/kuroshio_stream/kuroshio_stream.html\)\). Shaded periods with latitude \$< 31.8^{\circ}\text{N}\$ denote the LM state of the Kuroshio designated by JMA. As we noted in introduction, the LM occurrences and durations are highly irregular. During the satellite altimeter era after 1992, one LM event took place in mid-2004 and lasted for 14 months. Following this short-lived event and a dormant period of 12 years, an intense and more persistent LM event initiated in August 2017 \(Qiu 2019; Sugimoto et al. 2020\) and the event is still ongoing at the writing of this article.](https://www.</p>
</div>
<div data-bbox=)

Due to the lack of persistent LM occurrence in the past three decades, the KE dynamic state, as shown in Fig. 4, has been dominated by the decadal variability whose time scale is dictated by the negative feedback loop between the KE and overlying atmospheric storm track interactions. Indeed, this wind-forced KE variability was operative in the beginning of 2017 when the KE switched from a stable dynamic state to a negative one following the PDO phase change in early 2014 (Fig. 4d). After its dynamic state entered the unstable phase, Fig. 6b reveals that the Kuroshio path along 140°E shifted southward over the shoaling Izu Ridge, resulting in fluctuating KE paths southeast of Japan (Qiu and Chen 2005, their section 5). Subsequent to the LM occurrence in August 2017, however, the offshore detouring Kuroshio becomes confined to the west of the Izu Ridge and its outflow is restricted to enter the open Pacific through a narrow but deep (depth > 1100 m)

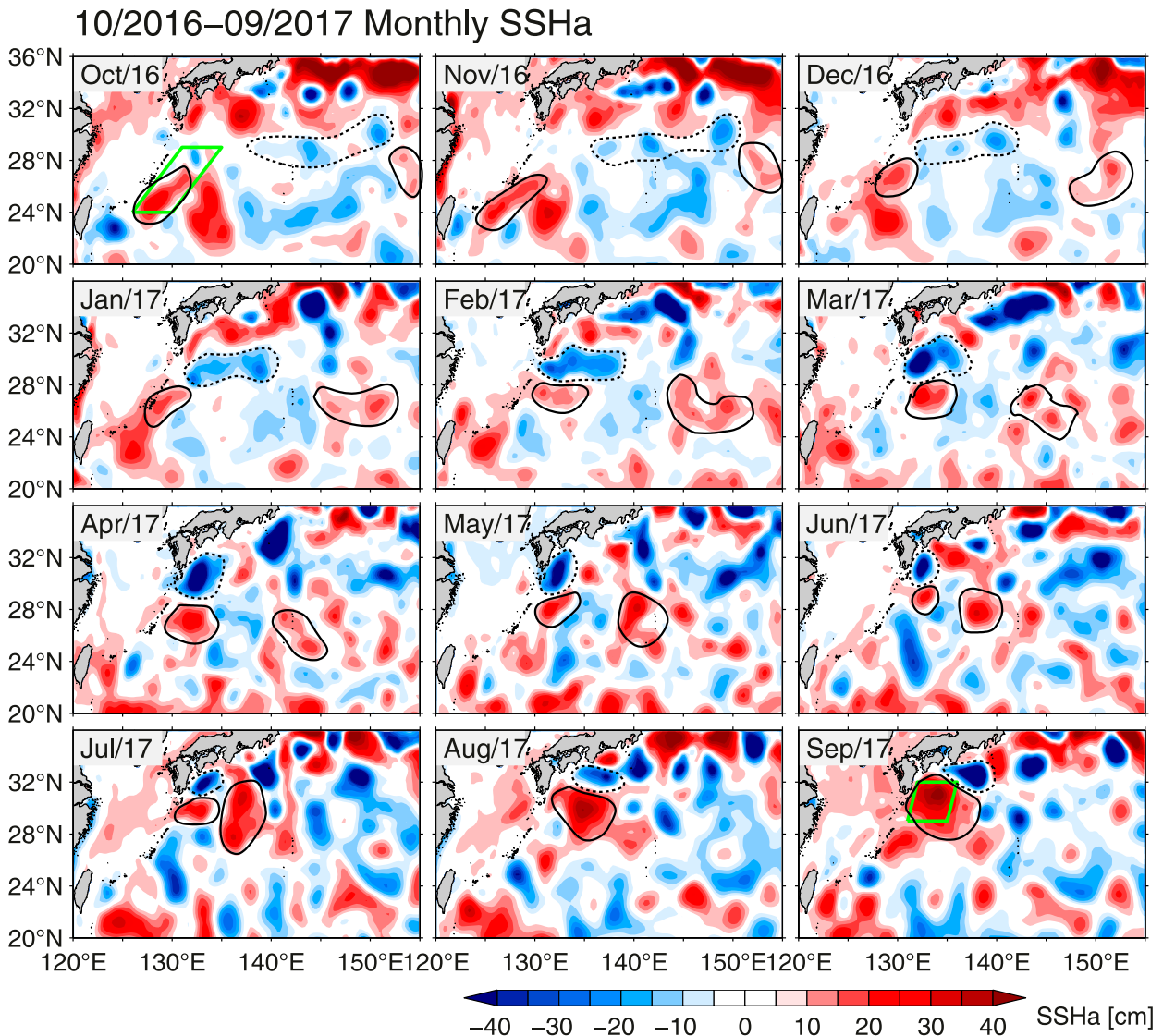


FIG. 7. Monthly maps of SSH anomalies from October 2016 to September 2017 in the western North Pacific Ocean. To avoid large-scale steric height changes due to seasonal heating/cooling, the area mean SSH anomaly value of each month is removed. Dashed lines denote the evolution of the trigger meander that appeared southeast of Kyushu in April 2017 and solid lines, the positive SSH anomalies that replaced the trigger meander off Kyushu in August 2017. The green box in the first (last) panel denotes the area used to construct the SSH anomaly time series shown in Figs. 8b and 8a.

channel between the mainland Japan and offshore Izu Ridge (see Fig. 6c; Kawabe 1985). Forced by these changes in the upstream Kuroshio, the KE jet in the 140°–153°E segment becomes stabilized, leading to the reversal of the KE index in 2018–19 as indicated in Figs. 4a and 4b.

Given the capability of the Kuroshio path south of Japan in reversing the KE dynamic state, a question arising naturally is what led to the occurrence of the 2017 LM event. To address this question, it is instructive to examine the evolution of the SSH anomaly field prior to the occurrence of the LM event. As depicted in Fig. 7, the LM is well developed by September 2017 and its presence corresponds geostrophically to the negative SSH anomaly (indicated by dashed line in the figure) located to

the south of Japan. Tracing it backward in time, it is discernible that this negative SSH anomaly initiated in the upstream Kuroshio southeast of Kyushu during April–May 2017 and it can be further traced back to around 145°–150°E in the 28°–30°N band as a sequence of cyclonic mesoscale eddies in October 2016. These cyclonic eddies propagated westward at a speed of 0.11 m s^{-1} during November 2016–March 2017 and consolidated into a single negative SSH anomaly off Kyushu in April 2017.

The negative SSH anomaly appearing in the upstream Kuroshio southeast of Kyushu in April–May 2017 is known as the “trigger” meander in existing literature and its importance as a precursor to the LM occurrence has been recognized in

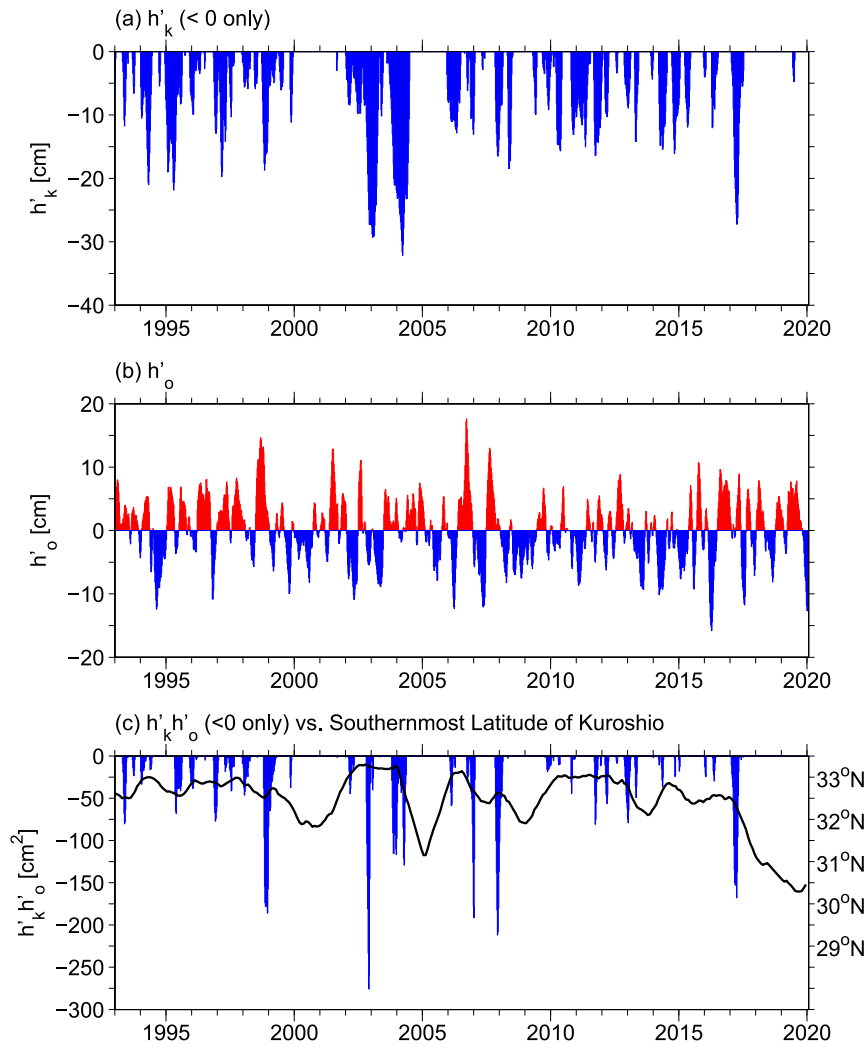


FIG. 8. (a) Time series of SSH anomalies averaged at southeast of Kyushu within a 4° width from 29° to 32°N . Only negative anomalies denoting the Kuroshio trigger meanders are shown. (b) Time series of SSH anomalies averaged in the 4° band east of the Ryukyu Islands from 24° to 29°N . (c) Product of the SSH anomalies shown in (a) and (b) with a lag of 4 months. Only negative anomalies denoting trigger meanders followed by positive SSH anomalies east the Ryukyu Islands are shown. The black line denotes the Kuroshio's southernmost latitude south of Japan.

many previous studies (e.g., Solomon 1978; Mitsudera et al. 2001; Ebuchi and Hanawa 2003; Miyazawa et al. 2004; Usui et al. 2008). In Fig. 8a, we plot the time series of the negative SSH anomalies averaged southeast of Kyushu within a 4° width from 29° to 32°N (the green box in last panel of Fig. 7) based on the altimeter SSH data. The negative SSH anomaly triggering the 2017 LM event corresponds to that appearing in early 2017. From this time series negative SSH anomalies, or trigger meanders, have appeared quite frequently off Kyushu during the past three decades. While a necessary condition, the trigger meander is clearly not a *sufficient* condition that will lead to a LM occurrence.

A careful inspection of the sequential SSH anomaly maps of Fig. 7 reveals another factor that has contributed to the 2017

LM event. Following the trigger meander in May 2017, Fig. 7 reveals that the area off Kyushu is replaced by an intense *positive* SSH anomaly in July and August. This positive SSH anomaly appears to have two sources: one originated from the STCC band of 24° – 27°N in October 2016 and moved subsequently northward to the east of the Ryukyu Islands, and the other started around 153°E in the 27° – 30°N band in October 2016 and moved westward to merge with the STCC-originated anomaly off Kyushu in August 2017 (see the solid lines in Fig. 7). An important role played by this intense positive SSH anomaly is that it is able to thrust the preceding negative SSH anomaly, or the trigger meander, eastward, leading it to develop into a LM south of Japan.

To examine if such positive SSH anomalies have succeeded other trigger meanders that appeared off Kyushu in the past, we construct in Fig. 8b the time series of the SSH anomalies averaged in the 4°-width band east of the Ryukyu Islands from 24° to 29°N (the green box in first panel of Fig. 7). As shown in Fig. 1, this band has an elevated SSH variance that connects the eddy-rich STCC to the Kuroshio southeast of Kyushu. The eddy variability in this band has positive and negative SSH anomalies with a time scale of typical oceanic mesoscales. To identify the events where a trigger meander southeast of Kyushu is followed by a positive SSH anomaly from east of the Ryukyu Islands, we multiply the SSH anomalies shown Fig. 8a to those of Fig. 8b with a lag of 4 months. Thus constructed, a negative product indicates an event in which a pre-existing trigger meander off Kyushu is succeeded by a positive SSH anomaly, with the magnitude of the product indicating their combined intensities. Figure 8c shows the time series of the above-mentioned negative product. Large negative products are now infrequent, and they appeared in late 1998, late 2002, late 2003–early 2004, late 2006, late 2007, and early 2017, respectively. When compared to the time series of the Kuroshio's southernmost latitude south of Japan (black curve in Fig. 8c), it is of interest to note that the large negative products of late 2002 and late 2003–early 2004 preceded the 2004–05 LM event, and the early 2017 large negative product preceded the 2017–present LM event. Although not categorized by JMA as LM events, the late 1998 large negative product preceded the offshore meandering of the Kuroshio in 1999–2000, and the large negative products of late 2006 and late 2007 preceded the offshore meandering of the Kuroshio in 2008–09.

We have from the above analyses identified the combined emergence of trigger meander and subsequent positive SSH anomalies southeast of Kyushu as a prerequisite for the LM development south of Japan. It is worth emphasizing that the importance of anticyclonic perturbations in facilitating trigger meanders off Kyushu to develop into a LM has been emphasized by a number of previous studies (Akitomo and Kurogi 2001; Kobashi and Hanawa 2004; Miyazawa et al. 2008; Usui et al. 2013; Tsujino et al. 2013). The origins of the anticyclonic perturbations proposed by these studies are, however, different from those identified in our analyses. All these previous studies have considered the anticyclonic perturbations of positive SSH anomalies to originate along the STCC band and be carried northward by the Kuroshio along the steep continental slope in the East China Sea. In light of the SSH anomaly maps shown in Fig. 7, we contend that the anticyclonic/positive SSH anomalies from the STCC band have more capacity and a direct route east of the Ryukyu Islands, rather than by deforming the slope-constrained Kuroshio in the East China Sea, to affect the trigger meander that develops off Kyushu. This contention of ours is also supported by the satellite altimeter data (Fig. 1) revealing that an elevated SSH anomaly band exists to the east of the Ryukyu Islands that connects the eddy-rich STCC to the time-varying Kuroshio south of Japan.

5. Impact on oceanic and atmospheric conditions

In the preceding section, we have quantified the impact of the 2017 LM event on the KE dynamic state based on altimeter-measured SSH information. To assess further the KE

change below the sea surface, we examine the in situ CTD data collected by JMA in the upstream KE region before and after the 2017 LM occurrence. Figure 9 compares the temperature, salinity, and cross-track geostrophic velocity profiles from the JMA's KS1702 cruise of March 2017 versus those from the RF1802 cruise of March 2018 (see Figs. 6b,c for locations of the CTD stations). From the T/S profiles, it is discernible that the KE front with the sharp T/S gradients in the 1000-m upper ocean shifted from 33.5°N in March 2017 to 34.5°N in March 2018. Accompanied by this northward shift is an increase in the KE's transport and intensity: the maximum eastward geostrophic velocity and transport of the KE jet referenced to 2000 dbar were 0.70 m s^{-1} and 70.2 Sv , respectively, from the 2017 cruise (Fig. 9c) and these values increased to 0.88 m s^{-1} and 76.3 Sv during the 2018 cruise (Fig. 9f).

Another noticeable difference between the two cruises is that the condition surrounding the KE jet was more variable in 2017 than in 2018. For example, Fig. 9a indicates the presence of an intense cold-core eddy centered around 30.5°N in 2017. This cold-core eddy has a geostrophic transport of 50 Sv , close to 70% of the KE's eastward transport value. Next to the coast of Japan, there appears a shallow branch of warmer/saltier subtropical-origin water in Figs. 9a and 9b. A look at the sequential SSH maps (not shown) indicates that it was a remnant of the KE jet before its main body shifted southward in early 2017. Accompanying this southward shift of the KE jet, a fresh, subarctic-origin water mass with salinity $< 34.0 \text{ psu}$ is seen to intrude to the north of the KE jet near 34°N (Fig. 9b). In contrast to the 2017 result, oceanic condition surrounding the KE jet was devoid of mesoscale perturbations in 2018. The above results from the subsurface CTD measurements regarding the LM-induced changes in the KE's position, intensity, and surrounding conditions, are all consistent with those of the preceding sections based on the altimeter SSH measurements.

To evaluate if the 2017 LM-induced KE change exerted a similar impact upon the overlying atmosphere as that of the wind-forced dynamic state change in the past three decades, we plot in Fig. 10a the surface turbulent heat flux anomaly field averaged in the two years of September 2017–August 2019 after the 2017 LM occurrence (this 2-yr window is selected because it is sufficiently long and contains two full seasonal cycles after the 2017 LM that are currently available to us). In conjunction with the northward shift and intensification of the KE jet, the surface turbulent heat fluxes exhibit positive anomalies (i.e., more heat supply from ocean to atmosphere) in the broad region east of Japan. This surface turbulent heat flux anomaly pattern is similar to that in Fig. 5a, showing the surface turbulent heat flux anomalies regressed to the KE index in January 1979–July 2017 before the 2017 LM. In Figs. 10b and 10c, we plot the storm track anomalies inferred from the lower tropospheric Eady growth rate and 850-hPa synoptic-scale transient eddy $\langle v'T' \rangle$ anomalies, in the two years after the 2017 LM occurrence. Consistent with the turbulent heat flux anomaly pattern shown in Fig. 10a, there exist an enhancement and a northward migration of the storm track activities in the recent two years. A comparison with Figs. 5b and 5c indicates that a very similar storm track response to the KE change was detected in the 1979–2017 period prior to the 2017 LM event.

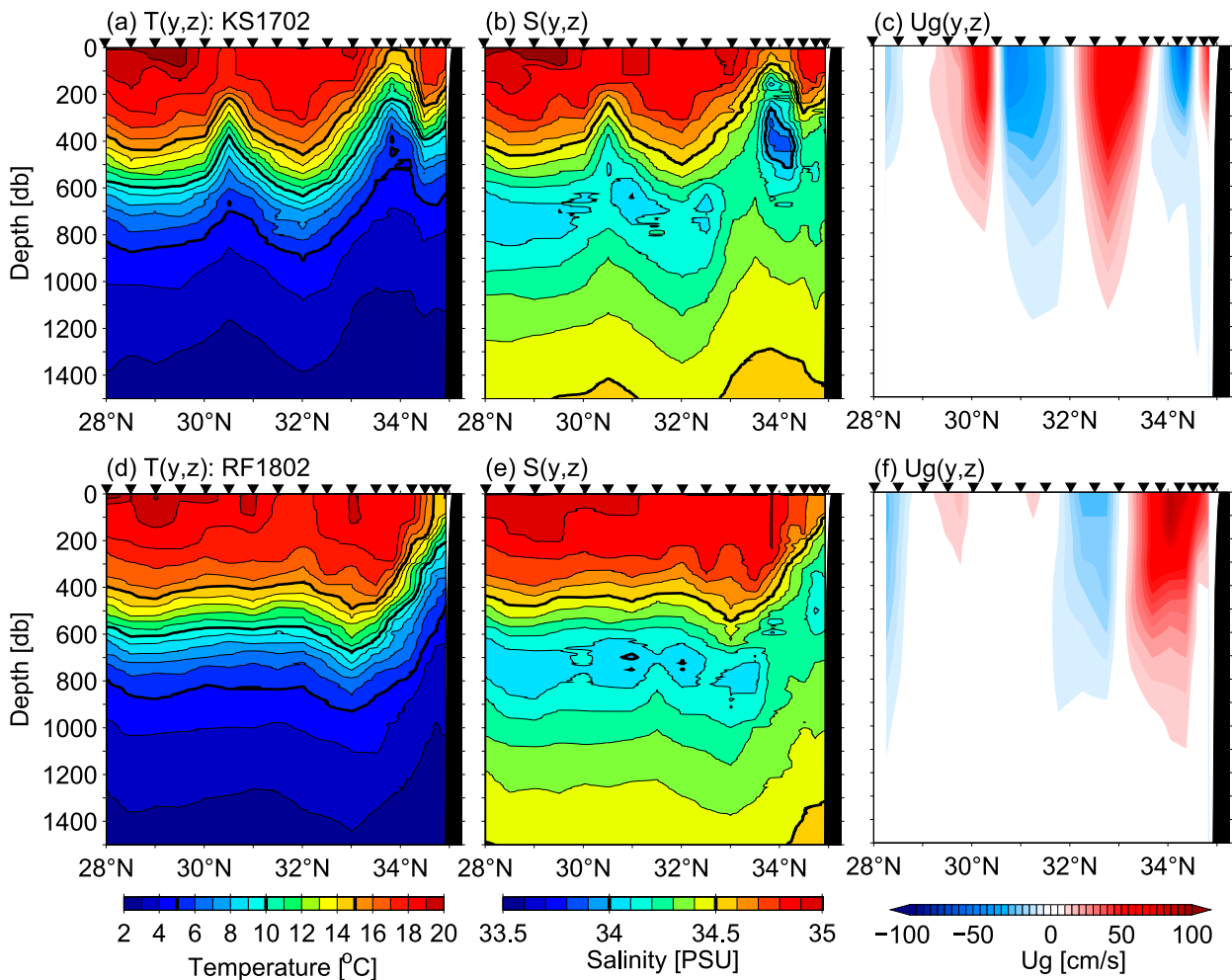


FIG. 9. Cross section profiles of (a) temperature, (b) salinity, and (c) geostrophic flows (referenced to 2000 dbar) from the JMA cruise KS1702 of 28 Feb–11 Mar 2017. (d)–(f) As in (a)–(c), but from the JMA cruise RF1802 of 2–12 Mar 2018.

Given the good agreement between the surface turbulent heat flux and storm track activity anomalies, it is of no surprise to find that a favorable correspondence also exists between the KE-induced w_{Ek} anomalies before and after the 2017 LM occurrence (cf. Figs. 10d and 5d). In short, the above comparisons indicate that the LM-induced KE variability after 2017 has exerted an impact upon the overlying atmospheric circulation similar to that by the wind-forced KE variability of the past three decades.

6. Discussion

Although the focus of our present study is on the recent interruption of the wind-forced decadal KE variability by the 2017 LM event, it is helpful to relate the KE dynamic state, the Kuroshio LM, and the basin-scale atmospheric variability from a longer time scale perspectives.

a. Oceanic reach of the decadal KE variability

In section 3, we combined four properties of the KE and defined the KE index to concisely describe the variations of the

KE dynamic state. Although all these four properties are based on characteristics of the observed KE jet/recirculation gyre west of 165°E, it does not imply that the oceanic influence of the decadal KE variability is confined regionally to the west of 165°E. Figure 11a shows the altimeter-measured SSH anomaly distribution regressed to the KE index during the 1993–2019 period. With the anomalous SSH signals being a good proxy for the upper heat content anomalies (Kelly et al. 2010), it is clear from Fig. 11a that the positive heat content anomalies during the stable state of KE extend both eastward beyond 165°E and northeastward into the Oyashio Extension and subarctic frontal regions. This is so because as the KE flows eastward, it sheds mesoscale eddies and broadens its entity via northward bifurcations (Kida et al. 2015). In fact, our recent study reveals that the decadal Oyashio Extension variability along ~40°N and 153°–173°E is by and large dictated by the KE variability through northward shed eddies and bifurcated branches (Qiu et al. 2017; their Fig. 3). It is of interest to note that the spatial pattern of the turbulent heat flux anomalies regressed to the KE index (Fig. 5a) bears a close resemblance to that of Fig. 11a,

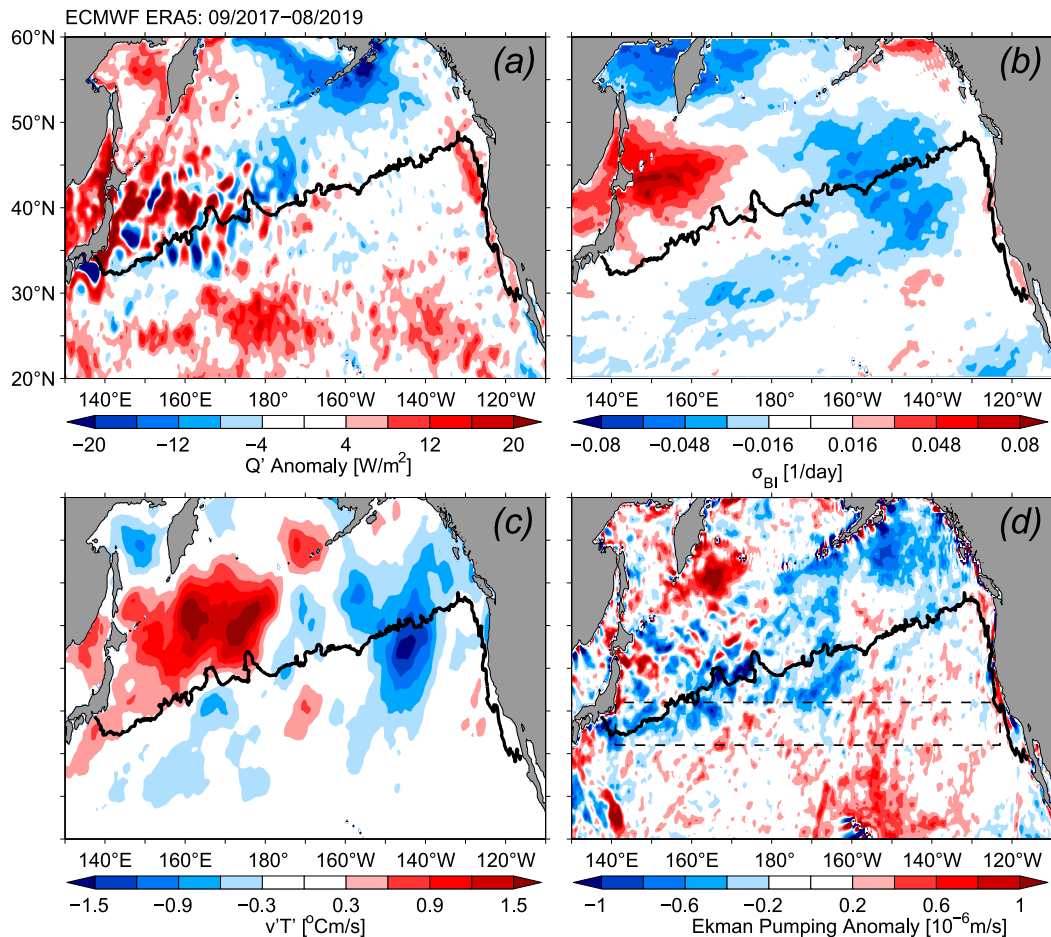


FIG. 10. Distributions of anomalous (a) surface turbulent heat flux, (b) maximum Eady growth rate at the 700–850-hPa level, (c) 2–8-day band-passed meridional transient eddy temperature heat flux at the 850-hPa level, and (d) Ekman pumping velocity fields averaged in the recent Kuroshio large meander period of September 2017–August 2019. With the mean SSH anomalies during this period equal to 0.05 m (see Fig. 4b), the color scale for each quantity can be converted to that shown in Fig. 5 by multiplying by 20. For example, a 10 W m^{-2} anomaly in (a) corresponds to a $200 \text{ W m}^{-2} \text{ m}^{-1}$ regression anomaly depicted in Fig. 5a.

lending credence to the idea that it is the KE-originated variability that is responsible for the diabatic heating anomalies presented in Fig. 5a.

b. Kuroshio LM and the PDO forcing

That the Kuroshio LM paths are able to steer the low-level cyclone tracks away from the southern coast of Japan has been previously observed by Nakamura et al. (2012). To clarify if the Kuroshio LMs affect the atmospheric circulation across the broader Pacific basin, we define the Kuroshio path index as anomalies of the Kuroshio southernmost latitude away from the coast of Japan (Fig. 12a). Thus defined, a positive anomaly indicates a LM state of the Kuroshio south of Japan. Figure 11b shows the turbulent heat flux anomalies regressed to the Kuroshio path index with a 2-month lag during the 1979–2019 period. Consistent with the findings by Nakamura et al. (2012), the diabatic heating effects of the LM events are confined to the regions surrounding Japan and there appears to be no

systematic influence on the extratropical storm tracks across the North Pacific basin (figures not shown). This result indicates that although a LM event can alter the extratropical storm tracks by modifying the KE dynamic state as we found in section 5, changes by the Kuroshio paths alone may not be sufficient to induce the storm track variability across the North Pacific basin.

We have emphasized in section 4 the roles played by mesoscale eddies along the 18° – 25° N STCC band for the LM development. Previous studies have shown that the eddy activity level in the STCC band is modulated by the PDO-related wind forcing (Yoshida et al. 2011; Qiu and Chen 2013). Specifically, when the PDO is in positive phase, enhanced westerlies and trade winds over the western North Pacific generate a greater Ekman temperature flux convergence along the STCC band, causing a stronger upper ocean meridional temperature gradient and strengthening the vertically sheared STCC/NEC system. This enhanced current shear results in a stronger

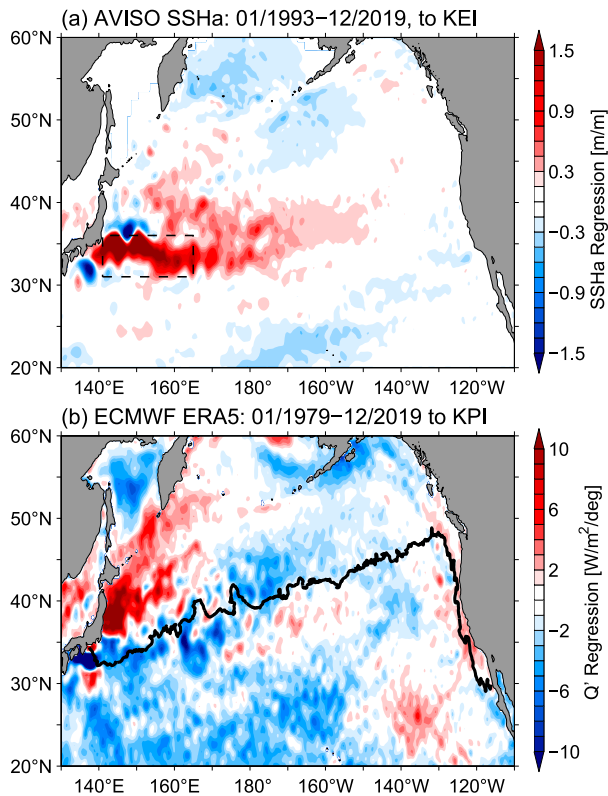


FIG. 11. (a) Regression map between the KE index and the North Pacific SSH anomaly field in 1993–2019. The dashed box denotes the region where the SSH anomalies are used to define the KE index shown in Fig. 4b. (b) Regression coefficient between the surface turbulent heat flux anomaly field and the Kuroshio path index of Fig. 12a with the former lagging the latter by 2 months. Thick black contour denotes the time-mean $w_{EK} = 0$ line.

baroclinic instability and elevates the level of regional eddy activities. A comparison between the Kuroshio path index and the PDO time series in Figs. 12a and 12b reveals that with the exception of the 1975 LM event, all other Kuroshio LM events were preceded by positive PDO phases. A lagged correlation analysis reveals that the Kuroshio path anomalies have a maximum correlation, $r = 0.27$, with the PDO index at a 32-month lag. Although not a high coefficient, this positive correlation is consistent with the notion that a positively phased PDO forcing is able to enhance the mesoscale eddy activities in the STCC band, conducive for the formation of the Kuroshio LMs. The 32-month lag likely reflects the time required for 1) the baroclinic instability along the STCC to fully grow, 2) the instability-generated eddies to propagate westward across the STCC and poleward along the Ryukyu Island, and 3) the development from a trigger meander off Kyushu to the LM south of Japan.

c. Imprint on PDO versus PMM by the KE variability

Throughout this study, we have emphasized the negative feedback mechanism that involves the KE dynamic state, the meridional migration of extratropical storm tracks/gyre-scale

Ekman pumping field, and the excitation of upper ocean baroclinic Rossby waves whose westward propagation alters the pre-existing KE dynamic state. Instead of invoking the storm track migration, Joh and Di Lorenzo (2019) have found recently that the decadal varying KE can induce an eastern Pacific wind stress curl response that projects on atmospheric forcing of the Pacific meridional mode (PMM; Chiang and Vimont 2004). Specifically, when it is in a stable state, the KE-induced positive w_{EK} anomaly shown in Fig. 5d in the 25° – 35° N band of the eastern North Pacific projects to the positive PMM forcing pattern (Fig. 13a). This PMM forcing can activate the central tropical Pacific El Niño–Southern Oscillation (CP-ENSO), which in turn can strengthen a positive PDO (or negative NPGO) forcing, generating the negative SSH anomalies in the eastern North Pacific and altering the KE to an unstable state after these wind-forced SSH anomalies reach the KE region.

It is important to note that both our study and that of Joh and Di Lorenzo (2019) advocate the negative feedback mechanism that favors the decadal climate variability involving the KE system. The difference lies in whether the KE-induced positive w_{EK} anomalies in the eastern North Pacific are a response confined to the midlatitude atmosphere via migration of storm tracks, or a response involving the tropical PMM/CP-ENSO variability. Figure 13b shows the spatial pattern of the w_{EK} anomaly regressed to the PDO index. Similar to the PMM-regressed pattern shown in Fig. 13a, the PDO-regressed pattern shows a positive w_{EK} anomaly in the eastern North Pacific that coincides with the positive w_{EK} anomaly identified in Fig. 5d. In other words, like their projection on PMM, the KE-induced w_{EK} anomalies project similarly on the PDO wind forcing pattern. The reason behind this similarity is because the PDO and PMM indices, as shown in Figs. 12b and 12c, share similar time-varying signals especially on the decadal time scale of our interest (see also Stuecker 2018). Given these results, we believe it will be challenging to differentiate the negative feedback mechanism described in this study and that proposed by Joh and Di Lorenzo (2019) from the statistical analyses alone. It will be crucial for future studies to clarify the atmospheric responses to the KE variability based on process-oriented, coupled ocean–atmosphere general circulation model simulations.

7. Summary

Low-frequency Kuroshio Extension variability is composed of concurrent changes in its latitudinal position, eastward transport, eddy kinetic energy level, and southern recirculation gyre strength. In its stable dynamic state, the KE has a northward position, an increased transport, a reduced eddy kinetic energy level, and an intensified recirculation gyre, and the opposite is true during its unstable dynamic state. In the past three decades, the KE has been observed to oscillate between these two dynamic states with a well-defined 10-yr period. The dominance of this decadal oscillation is caused by the delayed negative feedback mechanism, in which the KE variability is driven by the basin-scale wind forcing with its center over the eastern North Pacific and the forced KE, in turn, modifies the

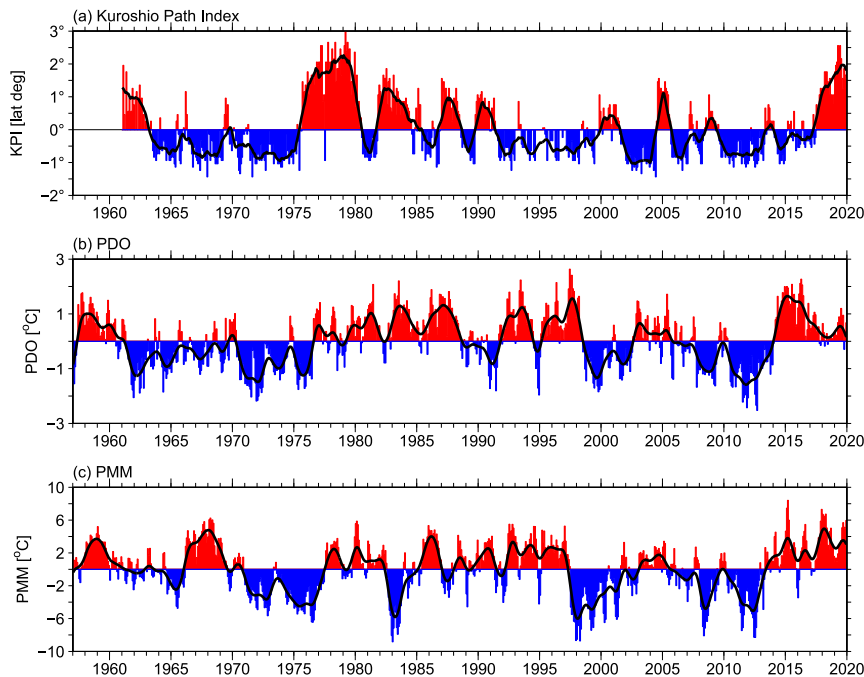


FIG. 12. (a) Time series of Kuroshio path anomalies measured from the southern coast of Japan. (b) Time series of the PDO index provided by http://research.jisao.washington.edu/data_sets/pdo. (c) Time series of the PMM index provided by <http://www.aos.wisc.edu/~dvimont/MModes/Data.html>. In all figures, thick black lines denote the time series after a low-pass filter that has a half-power at 6 months.

overlying storm tracks and the large-scale wind pattern through anomalous turbulent heat fluxes from the ocean to atmosphere.

The long-term, wind-forced KE variability was disrupted in August 2017 due to the occurrence of the Kuroshio large meander south of Japan. Instead of remaining in the unstable dynamic state that started in early 2017 in response to the 2014 phase change of the PDO wind forcing, the KE transitioned abruptly to a stable state in late 2017. The occurrence of LM is found from satellite altimeter measurements and available in situ hydrographic surveys to impact the KE in two important ways. First, it forced the Kuroshio to enter the open North Pacific through a northerly deep channel close to Japan, causing the downstream KE path to shift northward. Second, by entering through the northerly deep channel, the Kuroshio avoided overriding the shoaling Izu Ridge and minimized the KE path fluctuations in the east of the Izu Ridge. Both of these effects worked to stabilize the KE dynamic state following the 2017 LM occurrence.

Over the past three decades when the wind-forced KE variability prevails, the Kuroshio LM occurrence has been rare. The LM event preceding 2017 took place from July 2004 to August 2005 and this LM event exerted little impact upon the wind-forced KE variability because it occurred when the KE was already in a stable dynamic state. In agreement with the previous studies, we found that the LM occurrences in 2004–05 and 2017–present were preceded by trigger meanders (represented by negative SSH anomalies) in the upstream Kuroshio

southeast of Kyushu. For trigger meanders off Kyushu to develop fully into a LM state, we found it is necessary that they be succeeded by intense anticyclonic, or positive, SSH anomalies that work to thrust the trigger meander eastward and stationary south of Japan. Most of these anticyclonic/positive SSH anomalies have their origins in the STCC band of 18°–25°N and, rather than being advected by the Kuroshio through the East China Sea, they are observed to propagate northward to the east along the Ryukyu Islands.

The LM-induced KE dynamic state change after late 2017 is found to affect the overlying storm tracks and the large-scale wind pattern the same way as those generated by the wind-forced KE change prior to the 2017 LM occurrence. This consistent atmospheric response implies that although disrupted temporarily, the negative feedback loop and the decadal modulating KE variability will likely resume once the current LM event terminates. It will be interesting to find out how long the current LM event will last and how the KE dynamic state will respond in the coming years to the LM-induced positive Ekman pumping anomalies in the 32°–36°N band over the eastern North Pacific Ocean.

Acknowledgments. This study was conducted while EO and SS were on their sabbatical visit to the University of Hawaii. Constructive comments made by four anonymous reviewers have significantly improved an early version of the manuscript. The ECMWF ERA-5 reanalysis data used in this study were accessed from <https://cds.climate.copernicus.eu/>, the JMA hydrographic

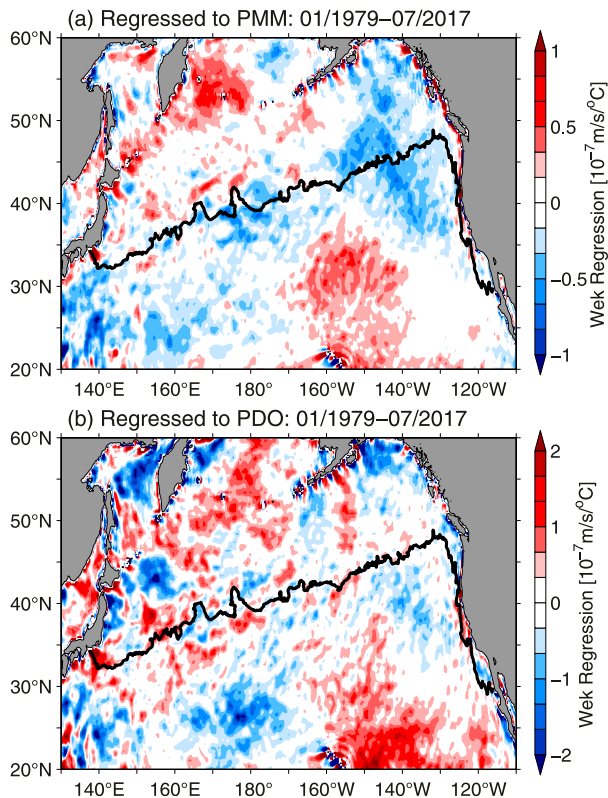


FIG. 13. Distributions of the w_{EK} anomalies regressed to (a) the PMM index of Fig. 12c and (b) the PDO index of Fig. 12b for the period of January 1979–July 2017. The thick black contour in both figures denotes the time-mean $w_{EK} = 0$ line.

cruise data and analysis information from <http://www.jma.go.jp/jma/indexe.html>, and the merged satellite altimeter data from Ssalto/Duacs and the Copernicus Marine and Environment Monitoring Service (<https://marine.copernicus.eu/>). We acknowledge the support of NSF Grant 2019312 and NASA Grant NNX17AH33G to BQ and SC, MEXT Grant 19H05700 and JSPS Grant 17K05652 to EO, and MEXT Grant 19H05704 and JSPS Grant 18K03737 to SS. This is SOEST Contribution Number 11158 and IPRC Contribution Number 1479.

REFERENCES

Akitomo, K., and M. Kurogi, 2001: Path transition of the Kuroshio due to mesoscale eddies: A two-layer, wind-driven experiment. *J. Oceanogr.*, **57**, 735–741, <https://doi.org/10.1023/A:1021292627245>.

Andres, M., J. H. Park, M. Wimbush, X. H. Zhu, K. I. Chang, and H. Ichikawa, 2008: Study of the Kuroshio/Ryukyu Current system based on satellite-altimeter and in situ measurements. *J. Oceanogr.*, **64**, 937–950, <https://doi.org/10.1007/s10872-008-0077-2>.

Bishop, S. P., F. O. Bryan, and R. J. Small, 2015: Bjerknes-like compensation in the wintertime North Pacific. *J. Phys. Oceanogr.*, **45**, 1339–1355, <https://doi.org/10.1175/JPO-D-14-0157.1>.

—, R. J. Small, F. O. Bryan, and R. A. Tomas, 2017: Scale dependence of midlatitude air–sea interaction. *J. Climate*, **30**, 8207–8221, <https://doi.org/10.1175/JCLI-D-17-0159.1>.

Booth, J. F., L. Thompson, J. Patoux, and K. A. Kelly, 2012: Sensitivity of midlatitude storm intensification to perturbations in the sea surface temperature near the Gulf Stream. *Mon. Wea. Rev.*, **140**, 1241–1256, <https://doi.org/10.1175/MWR-D-11-00195.1>.

Ceballos, L. I., E. Di Lorenzo, C. D. Hoyos, N. Schneider, and B. Taguchi, 2009: North Pacific Gyre Oscillation synchronizes climate fluctuations in the eastern and western boundary systems. *J. Climate*, **22**, 5163–5174, <https://doi.org/10.1175/2009JCLI2848.1>.

Cheng, Y.-H., C.-R. Ho, Q. Zheng, B. Qiu, J. Hu, and N.-J. Kuo, 2017: Statistical features of eddies approaching the Kuroshio east of Taiwan Island and Luzon Island. *J. Oceanogr.*, **73**, 427–438, <https://doi.org/10.1007/s10872-017-0411-7>.

Chiang, J. C. H., and D. J. Vimont, 2004: Analogous Pacific and Atlantic meridional modes of tropical atmosphere–ocean variability. *J. Climate*, **17**, 4143–4158, <https://doi.org/10.1175/JCLI4953.1>.

Di Lorenzo, E., and Coauthors, 2008: North Pacific Gyre Oscillation links ocean climate and ecosystem change. *Geophys. Res. Lett.*, **35**, L08607, <https://doi.org/10.1029/2007GL032838>.

Ebuchi, N., and K. Hanawa, 2003: Influence of mesoscale eddies on variations of the Kuroshio paths south of Japan. *J. Oceanogr.*, **59**, 25–36, <https://doi.org/10.1023/A:1022856122033>.

Frankignoul, C., and N. Sennechael, 2007: Observed influence of North Pacific SST anomalies on the atmospheric circulation. *J. Climate*, **20**, 592–606, <https://doi.org/10.1175/JCLI4021.1>.

—, —, Y.-O. Kwon, and M. A. Alexander, 2011: Influence of the meridional shifts of the Kuroshio and the Oyashio Extensions on the atmospheric circulation. *J. Climate*, **24**, 762–777, <https://doi.org/10.1175/2010JCLI3731.1>.

Gilson, J., and D. Roemmich, 2002: Mean and temporal variability in Kuroshio geostrophic transport south of Taiwan (1993–2001). *J. Oceanogr.*, **58**, 183–195, <https://doi.org/10.1023/A:1015841120927>.

Hoskins, B. J., and P. J. Valdes, 1990: On the existence of stormtracks. *J. Atmos. Sci.*, **47**, 1854–1864, [https://doi.org/10.1175/1520-0469\(1990\)047<1854:OTEOST>2.0.CO;2](https://doi.org/10.1175/1520-0469(1990)047<1854:OTEOST>2.0.CO;2).

Ichikawa, H., H. Nakamura, A. Nishina, and M. Higashi, 2004: Variability of northeastward current southeast of northern Ryukyu Islands. *J. Oceanogr.*, **60**, 351–363, <https://doi.org/10.1023/B:JOCE.0000038341.27622.73>.

Imawaki, S., A. S. Bower, L. Beal, and B. Qiu, 2013: Western boundary currents. *Ocean Circulation and Climate—A 21st Century Perspective*, 2nd ed. G. Siedler et al., Eds., Academic Press, 305–338.

Jayne, S., and Coauthors, 2009: The Kuroshio Extension and its recirculation gyres. *Deep-Sea Res. I*, **56**, 2088–2099, <https://doi.org/10.1016/j.dsr.2009.08.006>.

Joh, Y., and E. Di Lorenzo, 2019: Interactions between Kuroshio Extension and central tropical Pacific lead to preferred decadal timescale oscillations in Pacific climate. *Sci. Rep.*, **9**, 13558, <https://doi.org/10.1038/s41598-019-49927-y>.

Kawabe, M., 1985: Sea level variations at the Izu Islands and typical stable paths of the Kuroshio. *J. Oceanogr. Soc. Japan*, **41**, 307–326, <https://doi.org/10.1007/BF02109238>.

—, 1995: Variations of current path, velocity, and volume transport of the Kuroshio in relation with the large meander. *J. Phys. Oceanogr.*, **25**, 3103–3117, [https://doi.org/10.1175/1520-0485\(1995\)025<3103:VOCPVA>2.0.CO;2](https://doi.org/10.1175/1520-0485(1995)025<3103:VOCPVA>2.0.CO;2).

Kelly, K. A., R. J. Small, R. M. Samelson, B. Qiu, T. M. Joyce, Y.-O. Kwon, and M. F. Cronin, 2010: Western boundary currents and frontal air–sea interaction: Gulf Stream and

- Kuroshio Extension. *J. Climate*, **23**, 5644–5667, <https://doi.org/10.1175/2010JCLI3346.1>.
- Kida, S., and Coauthors, 2015: Oceanic fronts and jets around Japan: A review. *J. Oceanogr.*, **71**, 469–497, <https://doi.org/10.1007/s10872-015-0283-7>.
- Kobashi, F., and H. Kawamura, 2002: Seasonal variation and instability nature of the North Pacific Subtropical Countercurrent and the Hawaiian Lee Countercurrent. *J. Geophys. Res.*, **107**, 3185, <https://doi.org/10.1029/2001JC001225>.
- , and K. Hanawa, 2004: Hydrographic features off the south-east coast of Kyushu during the Kuroshio small meanders: A case study for small meanders that occurred in 1994 and 1995. *J. Oceanogr.*, **60**, 645–661, <https://doi.org/10.1007/s10872-004-5758-x>.
- Kwon, Y.-O., M. A. Alenxader, N. A. Bond, C. Frankignoul, H. Nakamura, B. Qiu, and L. Thompson, 2010: Role of the Gulf Stream and Kuroshio–Oyashio systems in large-scale atmosphere–ocean interaction: A review. *J. Climate*, **23**, 3249–3281, <https://doi.org/10.1175/2010JCLI3343.1>.
- Lien, R.-C., B. Ma, Y.-H. Cheng, C.-R. Ho, B. Qiu, C. M. Lee, and M.-H. Chang, 2014: Modulation of Kuroshio transport by mesoscale eddies at the Luzon Strait entrance. *J. Geophys. Res. Oceans*, **119**, 2129–2142, <https://doi.org/10.1002/2013JC009548>.
- Ma, J., and Coauthors, 2016: Western boundary currents regulated by interaction between ocean eddies and the atmosphere. *Nature*, **535**, 533–537, <https://doi.org/10.1038/nature18640>.
- Ma, X., and Coauthors, 2015: Distant influence of Kuroshio eddies on North Pacific weather patterns. *Sci. Rep.*, **5**, 17785, <https://doi.org/10.1038/srep17785>.
- Mantua, N. J., S. R. Hare, Y. Zhang, J. M. Wallace, and R. C. Francis, 1997: A Pacific interdecadal climate oscillation with impacts on salmon production. *Bull. Amer. Meteor. Soc.*, **78**, 1069–1079, [https://doi.org/10.1175/1520-0477\(1997\)078<1069:APICOW>2.0.CO;2](https://doi.org/10.1175/1520-0477(1997)078<1069:APICOW>2.0.CO;2).
- Masunaga, R., H. Nakamura, T. Miyasaka, K. Nishii, and B. Qiu, 2016: Interannual modulations of oceanic imprints on the wintertime atmospheric boundary layer under the changing dynamical regimes of the Kuroshio Extension. *J. Climate*, **29**, 3273–3296, <https://doi.org/10.1175/JCLI-D-15-0545.1>.
- Minobe, S., A. Kuwano-Yoshida, N. Komori, S.-P. Xie, and R. J. Small, 2008: Influence of the Gulf Stream on the troposphere. *Nature*, **452**, 206–209, <https://doi.org/10.1038/nature06690>.
- Mitsudera, H., T. Waseda, T. Yoshikawa, and B. Taguchi, 2001: Anticyclonic eddies and Kuroshio Meander formation. *Geophys. Res. Lett.*, **28**, 2025–2028, <https://doi.org/10.1029/2000GL012668>.
- Miyazawa, Y., X. Guo, and T. Yamagata, 2004: Roles of mesoscale eddies in the Kuroshio paths. *J. Phys. Oceanogr.*, **34**, 2203–2222, [https://doi.org/10.1175/1520-0485\(2004\)034<2203:ROMEIT>2.0.CO;2](https://doi.org/10.1175/1520-0485(2004)034<2203:ROMEIT>2.0.CO;2).
- , T. Kagimoto, X. Guo, and H. Sakuma, 2008: The Kuroshio large meander formation in 2004 analyzed by an eddy-resolving ocean forecast system. *J. Geophys. Res.*, **113**, C10015, <https://doi.org/10.1029/2007JC004226>.
- Mizuno, K., and W. B. White, 1983: Annual and interannual variability in the Kuroshio Current system. *J. Phys. Oceanogr.*, **13**, 1847–1867, [https://doi.org/10.1175/1520-0485\(1983\)013<1847:AAIVIT>2.0.CO;2](https://doi.org/10.1175/1520-0485(1983)013<1847:AAIVIT>2.0.CO;2).
- Na, H., K.-Y. Kim, S. Minobe, and Y. N. Sasaki, 2018: Interannual to decadal variability of the upper-ocean heat content in the western North Pacific and its relationship to oceanic and atmospheric variability. *J. Climate*, **31**, 5107–5125, <https://doi.org/10.1175/JCLI-D-17-0506.1>.
- Nakamura, H., T. Izumi, and T. Sampe, 2002: Interannual and decadal modulations recently observed in the Pacific storm track activity and East Asian winter monsoon. *J. Climate*, **15**, 1855–1874, [https://doi.org/10.1175/1520-0442\(2002\)015<1855:IADMRO>2.0.CO;2](https://doi.org/10.1175/1520-0442(2002)015<1855:IADMRO>2.0.CO;2).
- , T. Sampe, Y. Tanimoto, and A. Shimpo, 2004: Observed associations among storm tracks, jet streams and midlatitude oceanic fronts. *Earth's Climate: The Ocean–Atmosphere Interaction, Geophys. Monogr.*, Vol. 147, Amer. Geophys. Union, 329–346.
- , A. Nishina, and S. Minobe, 2012: Response of storm tracks to bimodal Kuroshio path states south of Japan. *J. Climate*, **25**, 7772–7779, <https://doi.org/10.1175/JCLI-D-12-00326.1>.
- O'Reilly, C. H., and A. Czaja, 2014: The response of the Pacific storm track and atmospheric circulation to Kuroshio Extension variability. *Quart. J. Roy. Meteor. Soc.*, **141**, 52–66, <https://doi.org/10.1002/qj.2334>.
- Parfitt, R., and H. Seo, 2018: A new framework for near-surface wind convergence over the Kuroshio Extension and Gulf Stream in wintertime: The role of atmospheric fronts. *Geophys. Res. Lett.*, **45**, 9909–9918, <https://doi.org/10.1029/2018GL080135>.
- Pierini, S., 2014: Kuroshio Extension bimodality and the North Pacific oscillation: A case of intrinsic variability paced by external forcing. *J. Climate*, **27**, 448–454, <https://doi.org/10.1175/JCLI-D-13-00306.1>.
- Qiu, B., 1999: Seasonal eddy field modulation of the North Pacific Subtropical Countercurrent: TOPEX/POSEIDON observations and theory. *J. Phys. Oceanogr.*, **29**, 2471–2486, [https://doi.org/10.1175/1520-0485\(1999\)029<2471:SEFMOT>2.0.CO;2](https://doi.org/10.1175/1520-0485(1999)029<2471:SEFMOT>2.0.CO;2).
- , 2019: Kuroshio and Oyashio currents. *Encyclopedia of Ocean Sciences*, 3rd ed. J. K. Cochran, H. Bokuniewicz, and P. Yager, Eds., Academic Press, 384–394.
- , and W. Miao, 2000: Kuroshio path variations south of Japan: Bimodality as a self-sustained internal oscillation. *J. Phys. Oceanogr.*, **30**, 2124–2137, [https://doi.org/10.1175/1520-0485\(2000\)030<2124:KPVSOJ>2.0.CO;2](https://doi.org/10.1175/1520-0485(2000)030<2124:KPVSOJ>2.0.CO;2).
- , and S. Chen, 2005: Variability of the Kuroshio Extension jet, recirculation gyre, and mesoscale eddies on decadal time-scales. *J. Phys. Oceanogr.*, **35**, 2090–2103, <https://doi.org/10.1175/JPO2807.1>.
- , and —, 2010: Eddy–mean flow interaction in the decadal-modulating Kuroshio Extension system. *Deep-Sea Res. II*, **57**, 1098–1110, <https://doi.org/10.1016/j.dsr2.2008.11.036>.
- , and —, 2013: Concurrent decadal mesoscale eddy modulations in the western North Pacific subtropical gyre. *J. Phys. Oceanogr.*, **43**, 344–358, <https://doi.org/10.1175/JPO-D-12-0133.1>.
- , N. Schneider, and S. Chen, 2007: Coupled decadal variability in the North Pacific: An observationally constrained idealized model. *J. Climate*, **20**, 3602–3620, <https://doi.org/10.1175/JCLI4190.1>.
- , S. Chen, P. Hacker, N. Hogg, S. Jayne, and H. Sasaki, 2008: The Kuroshio Extension northern recirculation gyre: Profiling float measurements and forcing mechanism. *J. Phys. Oceanogr.*, **38**, 1764–1779, <https://doi.org/10.1175/2008JPO3921.1>.
- , —, N. Schneider, and B. Taguchi, 2014: A coupled decadal prediction of the dynamic state of the Kuroshio Extension system. *J. Climate*, **27**, 1751–1764, <https://doi.org/10.1175/JCLI-D-13-00318.1>.
- , —, and —, 2017: Dynamical links between the decadal variability of the Oyashio and Kuroshio Extensions. *J. Climate*, **30**, 9591–9605, <https://doi.org/10.1175/JCLI-D-17-0397.1>.
- Révelard, A., C. Frankignoul, N. Sennechal, Y.-O. Kwon, and B. Qiu, 2016: Influence of the decadal variability of the Kuroshio Extension on the atmospheric circulation in the cold season. *J. Climate*, **29**, 2123–2144, <https://doi.org/10.1175/JCLI-D-15-0511.1>.

- Rio, M.-H., S. Guinehut, and G. Lamico, 2011: New CNES-CLS09 global mean dynamic topography computed from the combination of GRACE data, altimetry, and in situ measurements. *J. Geophys. Res.*, **116**, C07018, <https://doi.org/10.1029/2010JC006505>.
- Sasaki, Y. N., S. Minobe, and N. Schneider, 2013: Decadal response of the Kuroshio Extension jet to Rossby waves: Observation and thin-jet theory. *J. Phys. Oceanogr.*, **43**, 442–456, <https://doi.org/10.1175/JPO-D-12-096.1>.
- Small, R. J., R. A. Tomas, and F. O. Bryan, 2014: Storm track response to ocean fronts in a global high-resolution climate model. *Climate Dyn.*, **43**, 805–828, <https://doi.org/10.1007/s00382-013-1980-9>.
- Smirnov, D., M. Newman, M. A. Alexander, Y.-O. Kwon, and C. Frankignoul, 2015: Investigating the local atmospheric response to a realistic shift in the Oyashio sea surface temperature front. *J. Climate*, **28**, 1126–1147, <https://doi.org/10.1175/JCLI-D-14-00285.1>.
- Solomon, H., 1978: Occurrence of small “trigger” meanders in the Kuroshio off southern Kyushu. *J. Oceanogr. Soc. Japan*, **34**, 81–84, <https://doi.org/10.1007/BF02109256>.
- Stuecker, M. F., 2018: Revisiting the Pacific meridional mode. *Sci. Rep.*, **8**, 3216, <https://doi.org/10.1038/s41598-018-21537-0>.
- Sugimoto, S., and K. Hanawa, 2009: Decadal and interdecadal variations of the Aleutian Low activity and their relation to upper oceanic variations over the North Pacific. *J. Meteor. Soc. Japan*, **87**, 601–614, <https://doi.org/10.2151/jmsj.87.601>.
- , B. Qiu, and A. Kojima, 2020: Marked coastal warming off Tokai attributable to Kuroshio large meander. *J. Oceanogr.*, **76**, 141–154, <https://doi.org/10.1007/s10872-019-00531-8>.
- Taguchi, B., S.-P. Xie, N. Schneider, M. Nonaka, H. Sasaki, and Y. Sasai, 2007: Decadal variability of the Kuroshio Extension: Observations and an eddy-resolving model hindcast. *J. Climate*, **20**, 2357–2377, <https://doi.org/10.1175/JCLI4142.1>.
- , H. Nakamura, M. Nonaka, N. Komori, A. Kuwano-Yoshida, K. Takaya, and A. Goto, 2012: Seasonal evolutions of atmospheric response to decadal SST anomalies in the North Pacific subarctic frontal zone: Observations and a coupled model simulation. *J. Climate*, **25**, 111–139, <https://doi.org/10.1175/JCLI-D-11-00046.1>.
- Tsujino, H., S. Nishikawa, K. Sakamoto, N. Usui, H. Nakano, and G. Yamanaka, 2013: Effects of large-scale wind on the Kuroshio path south of Japan in a 60-year historical OGCM simulation. *Climate Dyn.*, **41**, 2287–2318, <https://doi.org/10.1007/s00382-012-1641-4>.
- Usui, N., H. Tsujino, H. Nakano, and Y. Fujii, 2008: Formation process of the Kuroshio large meander in 2004. *J. Geophys. Res.*, **113**, C08047, <https://doi.org/10.1029/2007JC004675>.
- , —, —, and S. Matsumoto, 2013: Long-term variability of the Kuroshio path south of Japan. *J. Oceanogr.*, **69**, 647–670, <https://doi.org/10.1007/s10872-013-0197-1>.
- Wijffels, S. E., M. M. Hall, T. Joyce, D. J. Torres, P. Hacker, and E. Firing, 1998: Multiple deep gyres of the western North Pacific: A WOCE section along 149°E. *J. Geophys. Res.*, **103**, 12 985–13 009, <https://doi.org/10.1029/98JC01016>.
- Wilson, C., B. Sinha, and R. G. Williams, 2009: The effect of ocean dynamics and orography on atmospheric storm tracks. *J. Climate*, **22**, 3689–3702, <https://doi.org/10.1175/2009JCLI2651.1>.
- Yasuda, I., K. Okuda, and M. Hirai, 1992: Evolution of a Kuroshio warm-core ring—Variability of the hydrographic structure. *Deep-Sea Res.*, **39A**, S131–S161, [https://doi.org/10.1016/S0198-0149\(11\)80009-9](https://doi.org/10.1016/S0198-0149(11)80009-9).
- Yoshida, S., B. Qiu, and P. Hacker, 2011: Low-frequency eddy modulations in the Hawaiian Lee Countercurrent: Observations and connection to the Pacific decadal oscillation. *J. Geophys. Res.*, **116**, C12009, <https://doi.org/10.1029/2011JC007286>.
- Zhang, D., T. N. Lee, W. E. Johns, C.-T. Liu, and R. Zantopp, 2001: The Kuroshio east of Taiwan: Modes of variability and relationship to interior ocean mesoscale eddies. *J. Phys. Oceanogr.*, **31**, 1054–1074, [https://doi.org/10.1175/1520-0485\(2001\)031<1054:TKEOTM>2.0.CO;2](https://doi.org/10.1175/1520-0485(2001)031<1054:TKEOTM>2.0.CO;2).